Sustainable Energy, Grids and Networks 42 (2025) 101676

Contents lists available at ScienceDirect

Sustainable Energy, Grids and Networks

journal homepage: www.elsevier.com/locate/segan

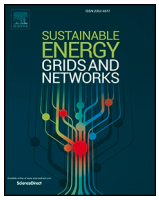

Optimal inertia allocation in future transmission networks: A case study on the Italian grid

Manuela Minetti [a,*], Matteo Fresia [a], Renato Procopio [a], Andrea Bonfiglio [a], Gio Battista Denegri [a], Giuseppe Lisciandrello [b], Luca Orrù [b]

[a] University of Genoa, Department of Electrical, Electronic, Telecommunications Engineering and Naval Architecture, Genoa, Italy
[b] Terna S.p.a., Rome, Italy

ARTICLE INFO

Keywords:
Transmission System
System Inertia
Grid Flexibilization

ABSTRACT

The paper introduces a technical-economic methodology to estimate the additional inertia required in a Transmission Network for future scenarios and presents an algorithm to optimally dispatch it among different sources and interwork busbars. First, the amount of inertia is calculated to constrain the Rate of Change of Frequency (RoCoF) within sustainable limits. Then, such inertia is allocated accounting for the contributions from Renewable Energy Sources (RESs) and Battery Energy Storage Systems (BESSs), complemented by the deployment of Synchronous Compensators (SCs) across various nodes of a Transmission Network. The methodology underwent testing within the Italian Transmission Network, utilizing the informational support furnished by the Italian Transmission System Operator (TSO). Despite its simplicity, the results exhibit notable accuracy, validated through rigorous comparisons with detailed time-domain simulations. Moreover, the low computational cost of the method, allowed a statistical analysis considering all the hours of year 2030, to get information on the distributions of the quantities of interest.

1. Introduction

1.1. Background and motivation

Electric networks are undergoing a rapid evolution, becoming complex and heterogeneous. The integration of Renewable Energy Sources (RESs), such as Photovoltaic (PV) units and Wind Turbines (WTs), and in general of inverter-based generation, such as Battery Energy Storage Systems (BESSs), into the traditional electric system is significantly increasing. Inverter-based generation is either replacing or supplementing conventional Synchronous Generators (SGs) like thermoelectric and hydroelectric generators. The increasing penetration of RESs has several consequences, including a decrease in the system's short-circuit power and a reduction in electric system inertia. The reduction of the system's primary regulating energy is significant, too. Focusing on the reduction of the overall inertia available in the system, it can be noted how frequency instability issues may arise during severe perturbations, especially regarding the Rate of Change of Frequency (RoCoF) [1–5].

In order to address this challenge, Transmission System Operators (TSOs) have implemented various measures for Frequency Support (FS), as required by the grid codes [1,6]. These include the deployment of Synchronous Compensators (SCs) and the implementation of enhanced control strategies for inverter-based generation. Traditionally, whether equipped with flywheels or not, SCs have been extensively utilized for this goal. These devices serve a dual role in enhancing the short-circuit power of the system and aiding in FS by mitigating the RoCoF, as shown in several studies [7–10].

On the other hand, in the last years, TSOs have updated the national grid codes, requiring RES power plants to participate in FS, to enhance the frequency stability of the systems. Synthetic Inertia (SI) is standing out as a rapidly advancing and promising application within the FS possible actions, offering a solution to address the issue of RoCoF degradation [11–15].

WTs need a proper control system in order to participate in FS, depending on the typology of generator. Examples of control schemes for the provision of SI for WTs can be found in [16–18] and in related references. These schemes involve the addition of a signal proportional to the frequency derivative within the active power channel, in order to keep the derivative of frequency within the desired range.

Few studies have been carried out considering SI provision by PV

* Corresponding author.
E-mail address: manuela.minetti@unige.it (M. Minetti).

https://doi.org/10.1016/j.segan.2025.101676
Received 14 June 2024; Received in revised form 10 February 2025; Accepted 2 March 2025
Available online 5 March 2025

Table 1
Comparative overview of the relevant literature.

Articles	SG inertial contribution	SC inertial contribution	PV	WT	BESS	Zonal repartition of inertial resources	COI RoCoF limitation	Zonal RoCoF limitation
[27]	✓	✓	×	×	×	×	✓	×
[28]	✓	✓	×	×	×	×	✓	×
[29]	✓	×	×	✓	×	×	✓	×
[31]	✓	✓	✓	✓	✓	×	✓	×
[32]	✓	✓	✓	✓	✓	×	✓	×
[33]	✓	✓	✓	✓	✓	×	✓	×
[34]	✓	✓	✓	✓	✓	✓	✓	×
This article	✓	✓	✓	✓	✓	✓	✓	✓

units. The authors of [19] provide an overview of the role of grid-scale PV plants in FS support. Some control schemes are proposed in [20] and [21,22].

The role of BESSs is relevant in the SI provision scenario because these devices are able to emulate inertia both in stand-alone and RES-coupled configuration. Examples of control schemes are proposed in [23–25] for utility-scale battery systems, while a demonstrative facility is presented in [26] for the small island of Pantelleria.

Despite existing a lot of literature regarding control schemes for application of SI to inverter-based generation, not so many studies address the issue of how much SI will be needed in transmission networks to comply with the requirements of the grid codes defined by the TSOs. Besides, few works provide a methodology to allocate the required inertia-delivering resources along the transmission networks.

1.2. Related works

In [27], a methodology is introduced to assess the required level of inertia at both national and zonal scales in order to control RoCoF, even in scenarios involving network separation. The study focuses on the Southern Australian network as a case study. However, this methodology does not consider the potential SI contribution deriving from RES generators. focusing only on the inertia provided by SGs and SCs.

Authors of [28] introduce a methodology for estimating the minimum requirements in terms of synchronous inertia for power systems with a significant integration of RESs. The methodology is specifically applied to a future scenario of the Australian National Electricity Market. However, again the methodology focuses only on SGs and SCs as sources of inertia, neglecting the possible FS contributions of RES power plants. Furthermore, the study does not propose a methodology for allocating the required synchronous inertia among the different market zones of the Australian network.

Reference [29] investigates the impact of RESs on the Croatian national grid, with a specific emphasis on issues related to RoCoF. The study demonstrates through simulations conducted in DIgSILENT PowerFactory [30] that the provision of SI by PV systems and WTs contributes to the limitation of RoCoF. However, it lacks a detailed examination about quantification of the share of RES that should contribute to SI provision and about how this share should be distributed among the different market zones of the Croatian grid.

The same shortcomings affect the analysis carried out in [31], that presents a technique to define the maximum non-synchronous generation of renewable energy by considering the minimum inertia of the power system. Indeed, it is not aimed at evaluating the possible allocation of inertial resources among the market zones.

1.3. Literature gap and contribution

Starting from this state of art, the novelty and the contribution of the present paper are the development of a methodology in evaluating the amount of additional inertia to be installed in each Italian market zone to keep the RoCoF of that market zone within the desired interval, as prescribed by National and European grid codes, after a codified disturbance. The inertia-providing sources that are considered are SCs, delivering “synchronous inertia”, and inverter-based generation (WTs, PV units and BESSs), with enabled SI services. It is highlighted that Terna S.p.A. (from now on “Terna”), the Italian TSO, has provided the dataset to validate the proposed procedure.

The authors of the present article have already addressed this issue in several studies. In [32,33], two different approaches for the quantification of the additional inertia to be provided through inverter-based resources and SCs at national level to limit the RoCoF of the transmission network Centre of Inertia (COI) are proposed. In the aforementioned studies, the considered transmission networks were handled as a single busbar system. Nevertheless, the allocation of the additional inertial resources among the market zones composing a transmission network was not discussed. This latter aspect was faced in [34]: therein, the methodology for the estimation of the additional inertia to be installed at zonal level is divided into two steps: at the first step, the National Algorithm (NA) is in charge of defining the amount of additional inertia to be provided by each source (PV units, WTs, BESSs and additional SCs) at national level in order to keep the RoCoF of the Italian COI within the desired range after a defined disturbance at national level (e.g., the loss of all the connections with the foreign neighbouring countries). The sources for the provision of additional inertia are selected in accordance with an economic indicator, in order to identify the best techno-economic mix.

Subsequently, a Zonal Algorithm (ZA) is in charge of the repartition of the share of additional inertia calculated at the first step among the Market Zones (MZ). The repartition is based on a criterion that considered the agglomeration of market zones in progressive “islands”, starting from the southernmost market zone and moving towards the northernmost one, with the purpose of sharing the additional inertia among MZ. The repartition is performed while minimizing the RoCoF of the progressive islands, with no constraints on the RoCoF of the single market zones, whose RoCoF might lay outside of the desired range: in fact, only the RoCoF of the Italian COI is limited. Moreover, the contingency that triggers the frequency transient in the ZA is the split between each isnad and the area at its northern boundary, which is in principle inconsistent with the one that originated the power imbalance at national level.

The new methodology proposed in the present paper aims to overcome the limitations of [34]. In fact, it is able to estimate the amount of additional inertia to be installed in each MZ to keep its RoCoF within the desired range.

This is done modelling each MZ as a single busbar network and estimating the contingency that originates the frequency transient linking it to the one experienced by the whole network. This allows to first determine the amount of inertia necessary to each MZ and, ex-post, the one needed by the whole network as the sum of all the contributions.

It is important to highlight that the strategy used in this study relies on a simplified model that achieves a beneficial trade-off between accuracy and computational efficiency; besides, the analysis is based on a large dataset, ensuring robustness. In order to validate the reliability of the results of the proposed approach, comparisons have been made with the results obtained from extensive simulations conducted in DIgSILENT PowerFactory, focusing on a specific subset of critical hours.

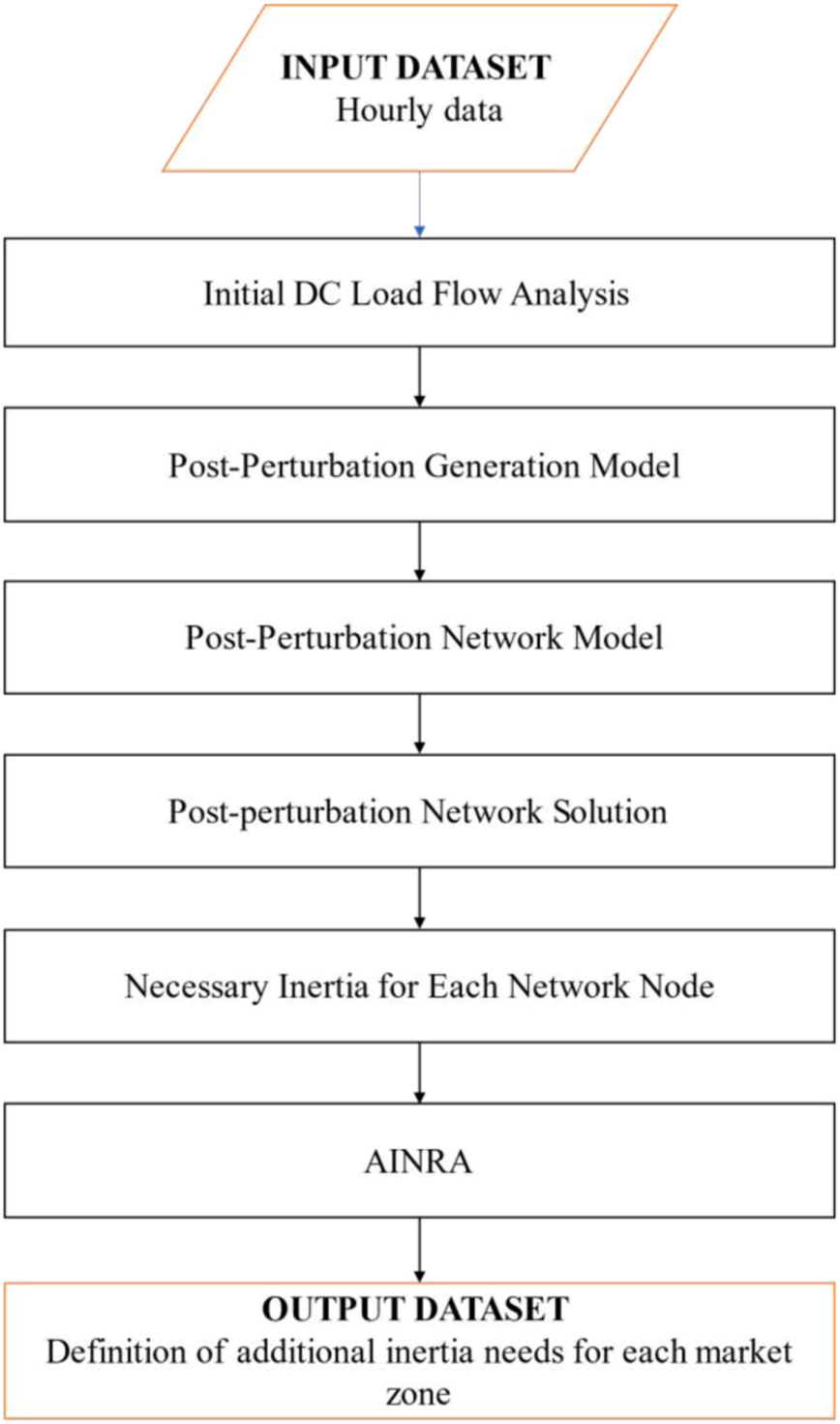

Fig. 1. Methodology scheme.

In Table 1, a comparison between the proposed study and the state-of-art references is shown, highlighting the main contribution of the present paper and the research gap.

The results of the proposed analysis will help the Italian TSO (but the approach can be easily applied to other TSOs) to quantify the need of additional inertia in the future scenario characterised by large inverter-based resources penetration. Moreover, the proposed tool splits the overall additional inertia among the available technologies and among the market zones, helping the TSO in analysing the possible investments to be performed to ensure reliable operation of the system.

The paper is structured as follows: Section II provides an introducing overview of the methodology; Section III fully details the mathematical model that has been developed to determine the needed amount of additional inertia and its allocation; Section IV describes dataset the authors have been provided with by Terna and the network test case; Section V and VI show respectively the validation procedure conducted in DIgSILENT PowerFactory and the results of the statistical analysis carried out over the whole 2030 year. Finally, some conclusive remarks and possible future developments are presented in Section VII.

2. Methodology overview

This section outlines the procedure to determine the additional inertia needed to control the RoCoF in a transmission network characterized by *N* nodes after a contingency event. The method is able to take into account various contingencies that affect the frequency profile of the grid nodes, such as load changes or generator and lines outages.

The input data for the procedure, which can be easily provided by the TSO, include two main components: i) model parameters about lines, SGs transient reactances and connection transformers and ii) working point data, which includes the active power demand of loads across all the *N* nodes, the generated active power at *N-1* nodes (excluding the slack node), specifications regarding the share of SGs that are connected to the network being "online" and information on active power flows on interconnection lines, both among Italian market zone and between Italian and foreigner market zones.

This delineation of inputs is essential for the procedure's effective operation and analysis of the power network.

The method's steps include:

i) Initial Direct Current Load Flow (DCLF) Analysis: since the transmission network is predominantly inductive, an initial DCLF analysis is conducted to determine the node voltage phases and the power supplied by the slack node. It is emphasized that an equivalent load and generator are supposed to be connected to each node to obtain an easily manageable model of the considered transmission network.
ii) Post-Perturbation Generation Model Definition: each generator is modelled as an equivalent voltage generator with a magnitude of 1 p.u. and a transient reactance provided by the TSO. It is highlighted that the voltage generator's phase at the post-perturbation instant remains consistent with the pre-contingency phase, in accordance with the phase invariance assumption detailed in the following section.
iii) Description of the Perturbation and the Post-Perturbation Network Model: the grid's configuration is updated according to the perturbation type, involving changes in absorbed powers, generator disconnections, line removals, or network separations.
iv) Post-Perturbation Network Solution: the aim is the evaluation of the post-perturbation generated powers at the N nodes with respect to the ones calculated in the initial conditions. Therefore, the active power produced by post-perturbation equivalent generators is calculated using the DCLF and considering the configuration obtained at step iii) and the post-perturbation generation model of step ii).
v) Identification of Inertia Requirements for Each Network Node: this step involves evaluating the inertia required at each node to maintain the RoCoF in the range [-0.5, 0.5] Hz/s after the contingency. Moreover, the amount of additional inertia that the new SCs and inverter-based generations must provide in addition to the conventional generation is defined.
vi) Steps i)-v) define the necessary inertia to cope with the contingency and will be described in detail in Section III-A
vii) Repartition of Additional Inertia Considering Inverter-Based Generations and New Synchronous Compensators: after identifying the required inertia, it can be distributed among different generator technologies using various strategies. This work proposes an algorithm, called Additional Inertia Nodal Repartition Algorithm (AINRA), to decide the amount of inertia each source will be committed to provide in each equivalent node.

For sake of simplicity, the methodology is summarized in Fig. 1.

3. Necessary inertia estimation and repartition algorithm

A. Necessary Inertia Estimation Procedure

This section presents the procedure developed to determine the amount of inertia needed to limit RoCoF in a transmission network of *N* nodes following a contingency.

In general, the *i*-th node is characterized by an equivalent load and an equivalent generator, characterised respectively by the active power absorption $P_{L,i0}$ and generation $P_{G,i0}$. The latter groups the active power production of different generation technologies: thermoelectric generators, hydroelectric generators, PV plants, WT plants and BESSs. Specifically, the active power P_{i0} injected into bus i in the pre-perturbation conditions can be calculated as follows:

$$P_{i0} = P_{G,i0} - P_{L,i0} \tag{1}$$

As specified in Section 2, the input data of the procedure include i) model parameters: the matrix of the nodal susceptances of the network $[B_R]$, the transient reactances of the SGs, the size of the connection transformers and their the short-circuit voltage v_{cc} [%], and ii) working point data: the loads' active power demand at all *N* nodes and the generated active power at *N-1* nodes (excluding the slack node), the sizes of the connected "online" generators and the active power flows on interconnection lines. It should be noted that the TSO usually provides data on the produced, absorbed and connected power for each hour of the considered year. So, all the quantities are hour-dependent, but this explicit reference is omitted in what follows for the sake of readability. Indeed, in the proposed procedure, the analysis is carried out by referring to a specific hour and therefore the relevant subscript is omitted.

Being the transmission network predominantly inductive, the first step (step *i)* of Section 2) is to perform a DCLF analysis of the grid in the initial and pre-perturbation conditions, in order to determine the voltage phases δ_{i0} ($i = 1,\ldots,N\text{-}1$) at all the grid nodes with the exception of the slack one and to determine the power provided by the node chosen as slack node. In detail, the following relation is implemented for the i-th node:

$$P_{i0} = \sum_{j=1}^{N} B_{R,ij}\delta_{j0} \tag{2}$$

where $B_{R,ij}$ is the susceptance between bus i and bus j; δ_{i0} and δ_{j0} are the phase angles of the voltages at buses i and j, respectively.

The second step is to define the generation model at the instant immediately after the perturbation. The *i*-th equivalent generator is described as a voltage generator of amplitude 1 p.u., phase $\delta_{G,i}$ and equivalent transient reactance $x'_{Geq,i}$. It is noted that, for the study of dynamic issues and stability analysis, adopting the transient invariance assumption for a synchronous machine is appropriate in the first few seconds following a disturbance [35]. In the proposed procedure, the relation $\delta_{G,i}(0^+) = \delta_{G,i0}$ is valid for the synchronous machine dynamic response since the phase angle is a state variable.

The equivalent transient reactance $x'_{Geq,i}$ can be easily determined considering the parallel of the reactances of the generators connected to the *i*-th node. In specific, the TSO provides the transient reactances for each conventional generator at the *i*-th node, whereas the reactances of inverter-based generators are set equal to the per unit short circuit voltage of the connection transformer.

Considering the grid perturbation at $t = 0$, it is possible to assume, as already mentioned, that $\delta_{G,i}(0^+)$ is equal to $\delta_{G,i0}$, where $\delta_{G,i0}$ is given by:

$$\delta_{G,i0} = \delta_{i0} + (x'_{Geq,i} P_{G,i0}) \tag{3}$$

The third step of the procedure requires to modify the grid configuration according to the considered perturbation. In detail, load variations can be described by updating the absorbed powers at the nodes, loss of generation is described by fictitiously increasing the load absorption at the specified node and the line detachment is modelled cancelling the relevant susceptance. For this reason, from now on, the post perturbation susceptance matrix will be labelled as $[B_{Rp}]$.

The aim of the fourth step is to evaluate the variations of the generated powers $\Delta P_{G,i}$ at the N nodes, considering the post-perturbation power $P_{G,i}$ with respect to the initial conditions $P_{G,i0}$.

To evaluate the post-perturbation generation powers $P_{G,i}$, it is necessary to consider the post-perturbation grid configuration and use the DCLF Eq. (4).

$$P_i = \sum_{j=1}^{N} B_{Rp,ij} \delta_j \tag{4}$$

where $B_{Rp,ij}$ is the susceptance between bus i and bus j, P_i and δ_i are the post-perturbation power injected and the phase at *i-th* bus of the post-perturbation network. Specifically, P_i can be determined as:

$$P_i = P_{G,i} - P_{L,i} \tag{5}$$

where $P_{L,i}$ is the post-perturbation absorbed power at *i-th* bus.

The post-perturbation produced active power $P_{G,i}$ can be described by the DCLF relation as:

$$P_{G,i} = B_{G,i}\left(\delta_{G,i0} - \delta_i\right) \tag{6}$$

where $B_{G,i}$ are the entries of a vector containing the nodal susceptances of the generators and $\delta_{G,i0}$ is the voltage phase of the equivalent generator connected to bus i, determined with (3).

Considering (4)-(6), one obtains:

$$P_{G,i} = P_{L,i} + \sum_{j=1}^{N} B_{Rp,ji}\left[-\frac{P_{G,j} - B_{G,j}\delta_{G,j0}}{B_{G,j}}\right] \tag{7}$$

Relation (7) is manipulated obtaining:

$$\sum_{j=1}^{N}\left(\delta_{ij} + \frac{B_{Rp,ij}}{B_{G,j}}\right) P_{G,j} = \sum_{j=1}^{N} B_{Rp,ij}\delta_{G,j0} - P_{L,i} \tag{8}$$

where δ_{ij} denotes the Kronecker delta.

Solving system (8) allows to determine the active power produced by the equivalent generators in post-perturbation conditions.

The fifth step aims to determine the necessary inertia to maintain an acceptable RoCoF value at the grid buses.

Considering the swing equation, it is possible to obtain the necessary inertia H_i to limit the RoCoF at the i-th node in the transmission network:

$$H_i = \frac{P_{G,i} - P_{G,i0}}{2RoCoF_{\text{lim}}}. \tag{9}$$

After defining the necessary inertia that the generations must provide for each node of the network and for the considered time interval, it is possible to distribute the inertia among the different generation technologies according to the methodology described in paragraph B.

B. Additional Inertia Nodal Repartition Algorithm (AINRA)

The overall inertia H_i necessary to limit the RoCoF at the i-th node in the transmission network can be split into two contributions, as stated by (10). The first contribution is the one related to the physical inertia $H_{p,i}$ of conventional SGs and SCs already installed in 2030 at node i. Since this contribution could be smaller than H_i, another term is introduced: it is the additional inertia $H_{add,i}$ possibly necessary at node i to limit the zonal RoCoF. In formulas:

$$H_i = H_{p,i} + H_{add,i} \tag{10}$$

$H_{add,i}$ is defined as:

$$H_{add,i} = H_{add,SC,i} + H_{add,WT,i} + H_{add,ST,i} + H_{add,PV,i} \tag{11}$$

where $H_{add,SC,i}$ represents the additional inertia resulting from the installation of supplementary SCs at node i, while $H_{add,WT,i}$, $H_{add,ST,i}$ and $H_{add,PV,i}$ denote the SI contributions from WT plants, BESSs and PV units installed at node i, respectively. It has to be highlighted that the AINRA procedure assumes an immediate response from the regulators of the inverter-based resources, meaning that the inertia to be installed corresponds to the instantaneous contribution provided by each inverter-based technology. This approximation is considered valid due to the rapid response characteristic of inverters.

The section describes an algorithm aimed at optimizing the technical and economic arrangement necessary to achieve the targeted increase in system inertia $H_{add,i}$. This algorithm considers the incorporation of newly installed SCs and the upgrade of control systems in inverter-based resources through dedicated FS controllers.

To set up the optimization problem, it is necessary to establish limits on the additional inertia contributions from all sources. The strategy by which the SI limits are defined recalls the one proposed in the National Algorithm (NA) presented in [34]. However, it differs in that the limits are calculated for each node of the transmission network and not for the single-busbar model of the whole network under consideration. For this reason, this approach will be here briefly recalled. The SI boundaries for each source and each hour are determined by estimating the maximum available active power for SI provision service, separately for under-frequency and over-frequency transients, and supposing to use it to maintain the RoCoF at its upper/lower limit. Below, SI limits for PV systems, WT power plants, and BESSs are briefly defined. For more comprehensive details and insights, please refer to [34].

For PV systems, the SI coefficient $H_{PV,\max,i}$ (referred to the rating of the PV plant apparent power connected to the i-th node in the considered hour $A_{PV,on,i}$) can be calculated as follows:

$$H_{PV,max,i} = \begin{cases} \dfrac{\dfrac{P_{curt,i}}{A_{PV,on,i}} f_n}{2RoCoF_{lim}} & P_{G,i} - P_{G,i0} < 0 \\ \dfrac{\dfrac{P_{PV,i}}{A_{PV,on,i}} f_n}{2RoCoF_{lim}} & P_{G,i} - P_{G,i0} > 0 \end{cases} \tag{12}$$

where $P_{PV,i}$ is the active power injected by PV systems at node i and $P_{curt,i}$ is the PV curtailment power at node i expressed as:

$$P_{curt,i} = P_{PV,i,MPPT} - P_{PV,i}. \tag{13}$$

being $P_{PV,i,MPPT}$ the Maximum Power Point Tracking (MPPT) power of the PV source at node i. In other terms, the active power that is considered available for SI services is the curtailment power (thus, the possibly available ramp-up power) during underfrequency transients and the whole active power production during overfrequency transients (representing the maximum ramp-down power).

Concerning WT power plants, the SI coefficient $H_{WT,\max,i}$, expressed on the base of the apparent power rating of the WT plant connected to the i-th node during the specified hour $A_{WT,on,i}$, can be determined as follows:

$$H_{WT,\mathrm{maxi}} = \begin{cases} \dfrac{\Delta P_{WT,i}}{\dfrac{A_{WT,on,i}}{2RoCoF_{lim}}} f_n & P_{G,i} - P_{G,i0} < 0 \\ \dfrac{P_{WT,i}}{\dfrac{A_{WT,on,i}}{2RoCoF_{lim}}} f_n & P_{G,i} - P_{G,i0} > 0 \end{cases} \tag{14}$$

assuming knowledge of the active power production $P_{WT,i}$ from all the WT units connected to the i-th node of the network, along with the corresponding apparent power $A_{WT,on,i}$ and $\Delta P_{WT,i}$, the active power available for SI provision in under-frequency transient. In detail, considering the minimum power factor to be granted by WT power plants $\cos\varphi_{\min}$ and the converter overloading coefficient α, $\Delta P_{WT,i}$ can be calculated as:

$$\Delta P_{WT,i} = \sqrt{\alpha^2 A_{WT,on,i}^2 - P_{WT,i}^2 \frac{1-\cos^2\varphi_{min}}{\cos^2\varphi_{min}}} - P_{WT,i} \tag{15}$$

A comparable method is suggested for BESS, in which:

$$H_{ST,max,i} = \frac{\frac{\Delta P_{ST,i}}{A_{ST,on}} f_n}{2RoCoF_{lim}} \tag{16}$$

The difference lies in the definition $\Delta P_{st,i}$, which must account for the two-way power flow of the storage unit, as follows:

$$\Delta P_{ST,i} = \begin{cases} \sqrt{\alpha^2 A_{ST,on,i}^2 - P_{ST,i}^2 \dfrac{1-\cos^2\varphi_{\min}}{\cos^2\varphi_{\min}}} - P_{ST,i} & P_{G,i} - P_{G,i0} < 0 \\ \left| -\sqrt{\alpha^2 A_{ST,on,i}^2 - P_{ST,i}^2 \dfrac{1-\cos^2\varphi_{\min}}{\cos^2\varphi_{\min}}} - P_{ST,i} \right| & P_{G,i} - P_{G,i0} > 0 \end{cases} \tag{17}$$

where $A_{ST,on,i}$ represents the rating of BESS power plants connected to the network at node i, $P_{ST,i}$ represents the active power production of BESS power plants at node i (positive when power is injected into the network and negative when power is withdrawn from the network) and $\cos\varphi_{\min}$ is the minimum operational power factor for BESS power plants.

The objective function to be minimised is a linear economic objective function, accounting for the costs related to the provision of the additional inertia needed to limit the zonal RoCoF at the node i. It is expressed by (18):

$$Obj_i = C_{SC,i}\left(H_{add,SC,i}\right) + C_{WT,i}\left(H_{add,WT,i}\right) + C_{PV,i}\left(H_{add,PV,i}\right) + C_{ST,i}\left(H_{add,ST,i}\right) \tag{18}$$

where $C_{SC,i}$ represents the costs for the installation of additional SCs in the market zone i, while $C_{WT,i}$, $C_{PV,i}$ and $C_{ST,i}$ represent the cost for the upgrade of the controller of WT, PV and BESS power plants. The definition of these four economic terms is furtherly detailed in (19).

$$\begin{cases} C_{SC,i}\left(H_{add,SC,i}\right) = k_{SC} \cdot A_{SC,i} = k_{SC} \cdot H_{add,SC,i} \cdot \dfrac{S_b}{H_{SC}} \\ C_{WT,i}\left(H_{add,WT,i}\right) = k_{WT} \cdot \dfrac{A_{WT,i}}{A_{WT,tower}} = k_{WT} \cdot \dfrac{H_{add,WT,i}}{A_{WT,tower}} \cdot \dfrac{S_b}{H_{WT,max,i}} \\ C_{PV,i}\left(H_{add,PV,i}\right) = k_{PV} \cdot \dfrac{A_{PV,i}}{A_{PV,av}} = k_{PV} \cdot \dfrac{H_{add,PV,i}}{A_{PV,av}} \cdot \dfrac{S_b}{H_{PV,max,i}} \\ C_{ST,i}\left(H_{add,ST,i}\right) = k_{ST} \cdot A_{ST,i} = k_{ST} \cdot H_{add,ST,i} \cdot \dfrac{S_b}{H_{ST,max,i}} \end{cases} \tag{19}$$

where k_{SC} denotes the cost in Euros per MVA of a new SC, k_{WT} represents the expense related to the integration of a SI controller into a WT inverter, expressed in Euros per WT inverter, k_{PV} indicates the cost of incorporating a SI controller into a PV unit inverter, expressed in Euros per PV inverter, and k_{ST} accounts the cost of deploying an SI controller in a BESS inverter, expressed in Euros per MVA. $A_{WT,tower}$ and $A_{PV,av}$ correspond to the typical sizes in MVA of inverters connected to a WT and to a PV unit, respectively; finally, H_{SC} stands for the inertia constant of a single SC.

The optimization problem can be formally defined for the i-th node in the under-frequency and over-frequency cases. Under-frequency transient happens in the market zones where the generated power variation is negative (i.e. $P_{G,i} - P_{G,i0} < 0$), while over-frequency transient is characterized by a positive generated power variation (i.e. $P_{G,i} - P_{G,i0} > 0$). Therefore, the structure of the optimization problem, whose decision variables and input parameters are summarised in Appendix A, in case of under-frequency transient can be defined as:

$$\begin{aligned} &\min_{H_{add,PV,i},H_{add,WT,i},H_{add,ST,i},H_{add,SC,i}} Obj_i = \min_{H_{add,PV,i},H_{add,WT,i},H_{add,ST,i},H_{add,SC,i}} \left[C_{SC,i}\left(H_{add,SC,i}\right) + C_{WT,i}\left(H_{add,WT,i}\right) + C_{PV,i}\left(H_{add,PV,i}\right) + C_{ST,i}\left(H_{add,ST,i}\right)\right] \\ &s.t. \\ &P_{G,i} - P_{G,i0} = -2\left(H_i + H_{add,PV,i} + H_{add,WT,i} + H_{add,ST,i} + H_{add,SC,i}\right)\frac{RoCoF_{\lim}}{f_n} \\ &0 \le H_{add,WT,i} \le H_{WT,max,i}\frac{A_{WT,on,i}}{S_b} \\ &0 \le H_{add,ST,i} \le H_{ST,max,i}\frac{A_{ST,on,i}}{S_b} \\ &0 \le H_{add,PV,i} \le H_{PV,max,i}\frac{A_{PV,on,i}}{S_b} \\ &\forall i = 1 \ldots N \end{aligned} \tag{20}$$

On the other hand, the over-frequency case can be obtained by substituting $-RoCoF_{\lim}$ with $RoCoF_{\lim}$ in Eq. (20) and considering the corresponding upper limits for the SI coefficients. The structure of the optimization problem in case of over-frequency transient is:

$$\min_{H_{add,PV,i},H_{add,WT,i},H_{add,ST,i},H_{add,SC,i}} Obj_i = \min_{H_{add,PV,i},H_{add,WT,i},H_{add,ST,i},H_{add,SC,i}} \left[C_{SC,i}\left(H_{add,SC,i}\right) + C_{WT,i}\left(H_{add,WT,i}\right) + C_{PV,i}\left(H_{add,PV,i}\right) + C_{ST,i}\left(H_{add,ST,i}\right)\right]$$

$$s.t.$$

$$P_{G,i} - P_{G,i0} = 2\left(H_i + H_{add,PV,i} + H_{add,WT,i} + H_{add,ST,i} + H_{add,SC,i}\right)\frac{RoCoF_{\lim}}{f_n}$$

$$0 \le H_{add,WT,i} \le H_{WT,max,i}\frac{A_{WT,on,i}}{S_b} \tag{21}$$

$$0 \le H_{add,ST,i} \le H_{ST,max,i}\frac{A_{ST,on,i}}{S_b}$$

$$0 \le H_{add,PV,i} \le H_{PV,max,i}\frac{A_{PV,on,i}}{S_b}$$

$$\forall i = 1 \ldots N$$

The first set of constraints of (20) and (21) is the swing equation applied to the i-th node of the considered transmission network: here, the RoCoF is not considered as a decision variable but it is fixed at its limit value in order to avoid the non-linearity of the problem. This assumption is justified by the fact that, since the aim of the optimization problem is to limit the additional inertia provision's costs, the least expensive mix would be the one limiting the RoCoF at $RoCoF_{\lim}$ and not at values closer to 0.

The last three set of constraints of (20) and (21) limit the additional inertia that can be provided by the three inverter-based resources. The technical limits derived through (12), (14) and (16) are expressed on a local base (either $A_{WT,on,i}$, $A_{ST,on,i}$ or $A_{PV,on,i}$): for this reason, since the decision variables $H_{add,WT,i}$, $H_{add,ST,i}$ and $H_{add,PV,i}$ are expressed on the system base, a base change is performed through the multiplication by the term $\frac{A_{\rho,on,i}}{S_b}$, where subscript ρ denotes the inverter-based resource.

It is important to recall that, for each hour of considered year, N optimization problems are solved separately, one for each market zone.

Table 2
Generated power variations, hour 5686.

Network Node	$\Delta P_{G,i}$ [MW]
NORTH	9222.6
CENTRE-NORTH	531.6
CENTRE-SOUTH	185.1
SOUTH	51.6
CALABRIA	3.2
SICILY	3.9

In fact, as the optimization problem is defined, the formulation of the i-th optimization problem considers only decision variables pertinent to the i-th market zone. This assumption relies on the criterion applied to split the national contingency into N zonal contingencies, expressed for the i-th market zone as $P_{G,i} - P_{G,i0}$. Moreover, the limits on the SI contributions deliverable by inverter-based resources are assessed zone by

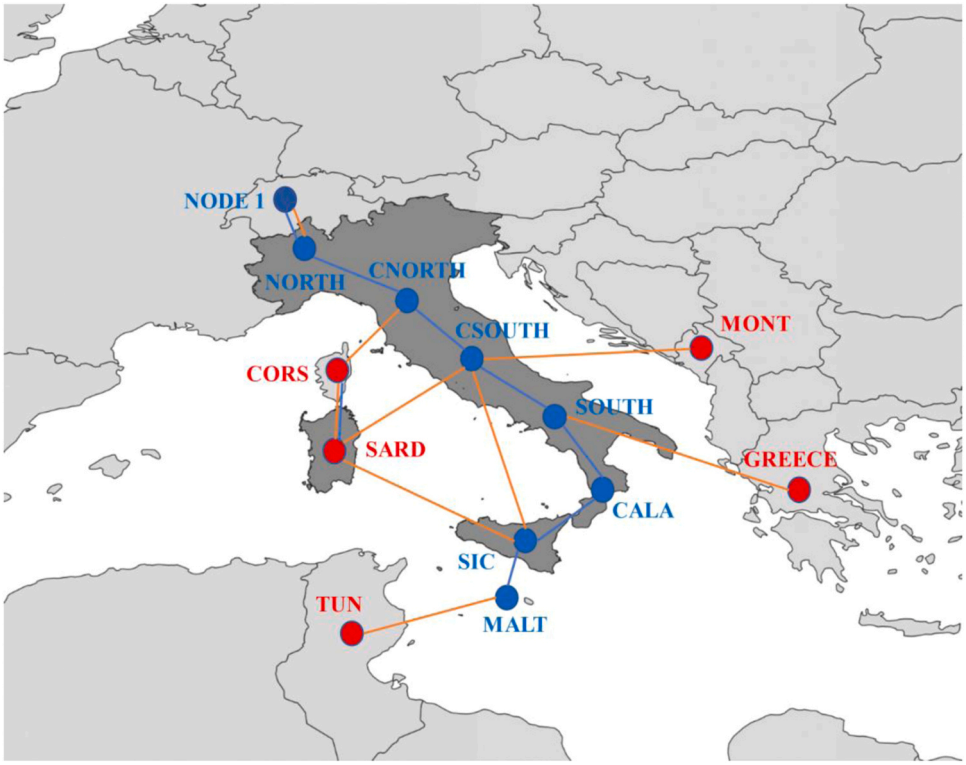

Fig. 2. The Italian market zones, AC transmission lines (blue lines) and HVDC transmission lines (orange lines).

Table 3
Needed and additional inertia, hour 5686.

Network Node	H_i [s]	$H_{add,i}$ [s]
NORTH	499.91	400.01
CENTRE-NORTH	461.13	20.91
CENTRE-SOUTH	26.58	0.62
SOUTH	9.25	0.00
CALABRIA	2.58	0.00
SICILY	0.16	0.00

Table 4
Distribution of the Additional Inertia, hour 5686.

Network Node	$H_{PV,i}$ [s]	$H_{WT,i}$ [s]	$H_{ST,i}$[s]	$H_{SC,i}$ [s]
NORTH	0.00	0.00	21.74	378.27
CENTRE-NORTH	0.00	0.01	0.98	19.93
CENTRE-SOUTH	0.00	0.62	0.00	0.00

zone and not on national base. Finally, having limited each zonal RoCoF to the limit value $RoCoF_{\text{lim}}$ following each zonal contingency, it is also ensured that the RoCoF of the transmission network COI is limited to $RoCoF_{\text{lim}}$ following the national contingency.

Table 5
Minimum values of RoCoF, hour 5686.

	RoCoF [Hz/s]		
Network Node	**Base scenario**	**ZA Frequency support**	**ZA Frequency support**
NORTH	−3.714	−1.523	−0.492
CENTRE-NORTH	−2.523	−0.824	−0.498
CENTRE-SOUTH	−0.533	−0.521	−0.491

4. Application of the methodology to the Italian transmission network

The provided approach underwent testing on the Italian Transmission Network. As outlined in reference [33], the Italian Transmission Network can be simplified the network can be simplified into the configuration shown in Fig. 2. In this representation, the network features a radial layout with 7 nodes: the one accounting for Europe, and the Italian Market Zones (MZ), i.e. North, Centre-North, Centre-South, South, Calabria, Sicily. It is important to note that the Sardinia market zone is connected to the mainland exclusively via HVDC links. In this methodology, Malta and Sardinia are modelled as absorptions or productions, linked to the Sicily and Centre-South nodes, respectively.

Terna S.p.A., the Italian Transmission System Operator (TSO), hereafter referred to as Terna, supplied extensive data for every hour (8760 hours) of the year 2030, as elaborated in [36]. This data encompasses load active power requests, the inertia constants for all rotating machines (SG and SC) envisaged in the 2030 network scenario, apparent power connected to the six nodes in each hour and the corresponding active power generated from all sources for each bus. Furthermore, the data include the elements of the nodal susceptances, the values of the synchronous reactances $x'_{G,i}$ and the transformers' data. It is important to note that the scenario's input data comprises sensitive information vital to the TSO: the dataset is developed based on historical load data and forecasting about the integration of emerging electricity-consuming technologies, such as electric vehicles and heat pumps. These demand profiles serve as inputs to a market analysis algorithm that determines the hourly generation dispatch needed to meet demand according to market regulation. The algorithm ensures the provision of dispatching services, including power reserve requirements, system security, and the resolution of potential congestion between market zones. Additionally, the algorithm simulates the Day-Ahead Market across Europe, predicting power exchanges between Italy and its neighbouring countries. Given that this algorithm has been developed internally by Terna, specific details, such as grid parameters and load flow assignments, are not disclosed. Some aggregated data can be

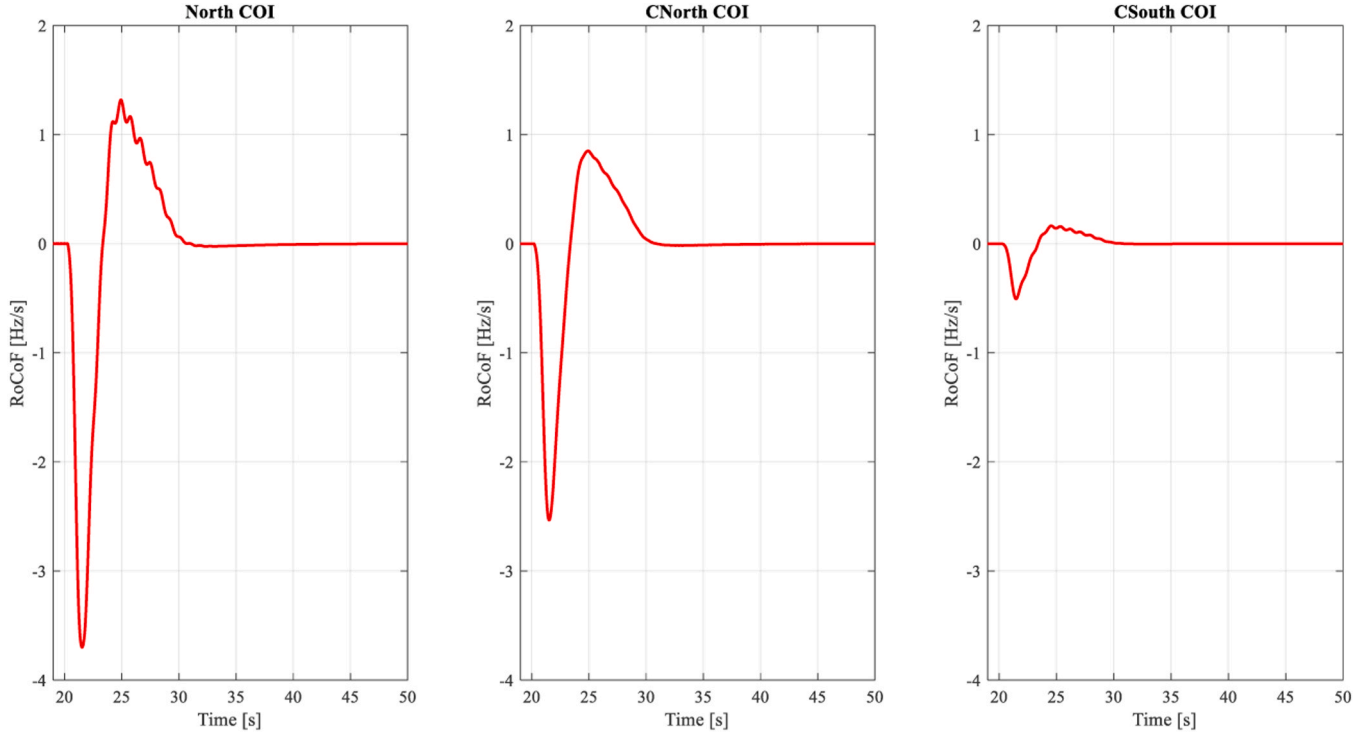

Fig. 3. RoCoF profiles with frequency support at North, Centre-North and Centre-South nodes.

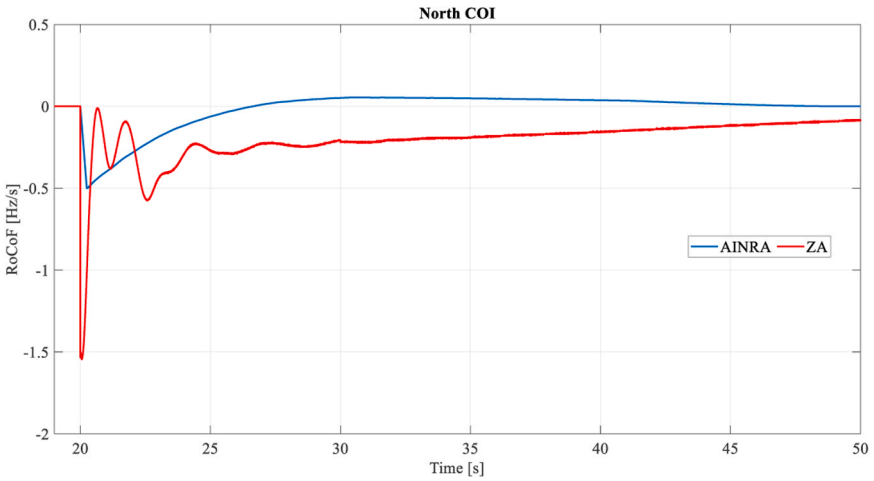

Fig. 4. RoCoF profiles with frequency support at North node – Comparison between the AINRA method and ZA.

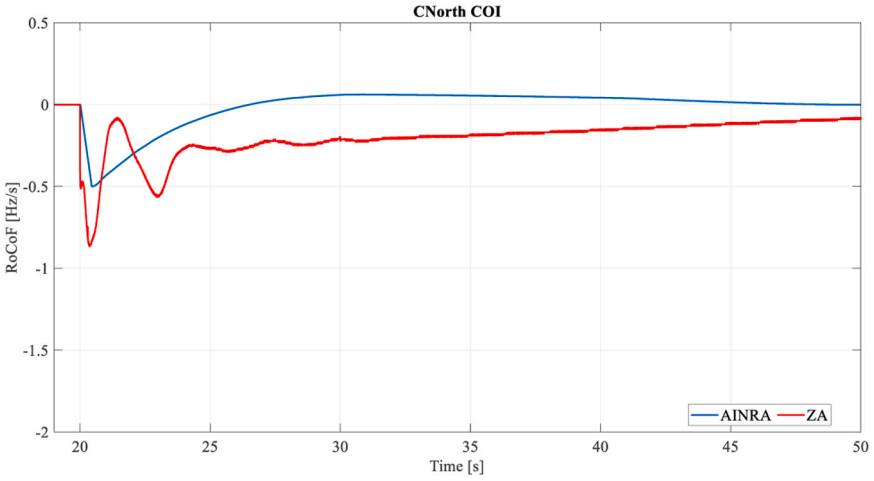

Fig. 5. RoCoF profiles with frequency support at Centre-North node – Comparison between the AINRA method and ZA.

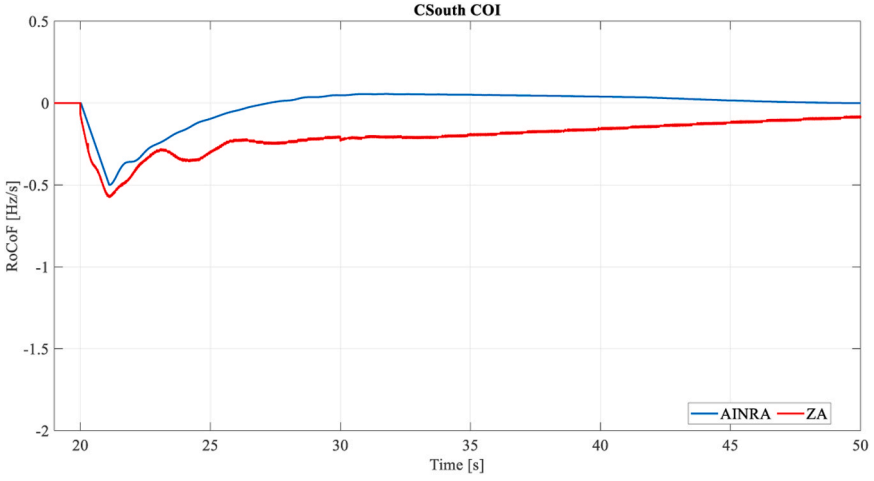

Fig. 6. RoCoF profiles with frequency support at Centre-South node – Comparison between the AINRA method and ZA.

found in the development plan of the Italian network [37].

The methodology was applied for all hours of the year 2030. The linear optimization problem has been solved applying a linear solver, namely *linprog*, embedded in Matlab. The computational time over the whole year was around 4 hours. Here the results of the 5686th hour of the year (i.e. 09:00 AM on August 13) are shown in detail, for the sake of brevity, while complete yearly results will be reported in section VI.

Commencing from the operational scenario at hour 5686, the Italian

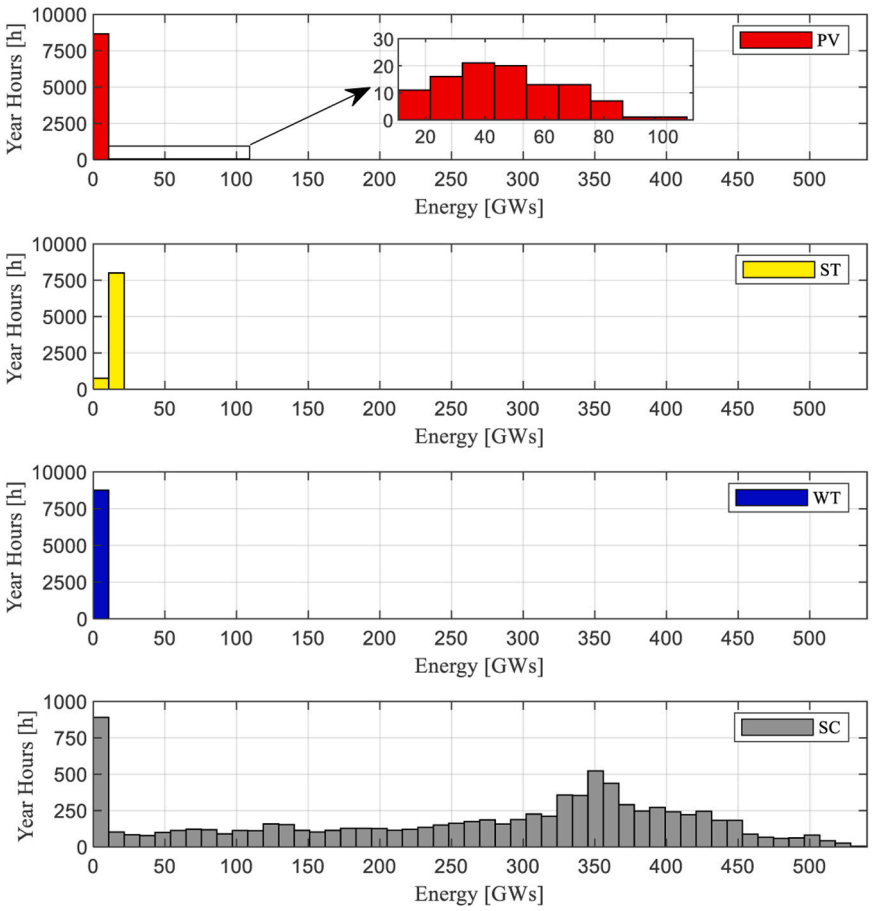

Fig. 7. Additional energy repartition at North node.

TSO necessitated examination of the potential separation of the Italian grid from the broader Continental Europe network. In particular, the occurrence triggering a variation in frequency was the loss of the 9998.1 [MW] power injection originating from Europe.

In accordance with the initial four steps elucidated in Section III, the power variations $\Delta P_{G,i}$ generated by the equivalent generators at each node in the Italian transmission network were determined, as reported in Table 2.

After determining the active power variations and using (8) it was possible to calculate the inertia H_i required to maintain a RoCoF of $\pm$ 0.5 Hz/s, as prescribe by the Italian grid code, and define the additional inertia $H_{add,i}$, to be added at each node when that of traditional generations is insufficient. In detail, the outcomes are presented in Table 3.

In conclusion, AINRA was used to distribute the additional inertia $H_{add,i}$ among inverter-based generations and SCs to be installed. The algorithm necessitates specific input data in the form of cost coefficients, namely k_{PV}, k_{WT}, k_{ST}, and k_{SC}. These coefficients have been provided by manufacturers and are not disclosed due to confidentiality constraints. Nonetheless, they align with ones presented in [36,38,39] and for explanatory purposes, their proportional relationships are as follows: k_{PV}: k_{WT}: k_{ST}:k_{SC}= 1:2:7:10.5.

The outcomes from AINRA, presented in Table 4, indicate that inertia support is predominantly needed at the North and Centre-North nodes. In these market areas, the installation of new SCs is deemed necessary, as the additional SI from inverter-based generators alone is insufficient to sustain a RoCoF of 0.5 Hz/s. A limited inertial support by WT power plants is required at market zone Centre-South. No inertial support is required at market zones South, Calabria and Sicily.

5. Validation of the developed method and simulation results

To enhance the reliability of the results, a validation process for a limited set of sample hours was carried out: in detail the simulation results of the 5686th are reported.

This validation procedure involves two dynamic simulations using DIgSILENT Power Factory and focuses on assessing the frequency transients following the loss of all the connections at the Italian northern border.

The first simulation was carried out assuming no inertial support from inverter-based generation and does not incorporate additional SCs. The second simulation involves the implementation of the results reported in Table 4 in DIgSILENT Power Factory, in order to verify whether the introduction of inertial support from WT, PV systems, BESSs, and the installation of new SCs can effectively limit the RoCoF of the within the desired range of [-0.5 Hz/s; 0.5 Hz/s] for each node. Furthermore, the AINRA results are compared with those of the Zonal Algorithm (ZA) proposed in [34] in order to highlight the differences.

According to Terna's data, each node is assumed to be connected to six equivalent SGs, which include various types of power plants including steam, gas, combined cycle, conventional hydro, pumped-storage, and run-of-river plants. These generators are equipped with governors and Automatic Voltage Regulators (AVRs), with their specific models obtained from the DIgSILENT PowerFactory Library [38]. Specifically, governor models are customized for each type of generator with details provided in [34]. Inverter-based generation is handled as static generation and is represented by modelling it as a current-controlled voltage source [39].

Each network node is equipped with three equivalent generators, representing PV, WT, and BESS power plants. To ensure the validation of

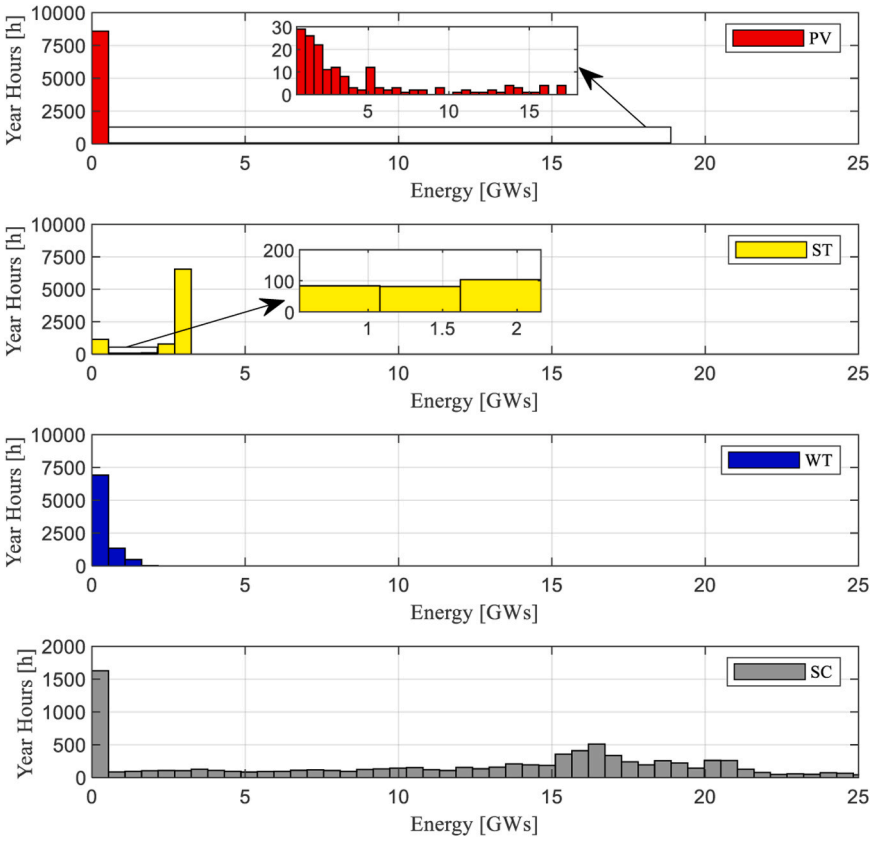

Fig. 8. Additional energy repartition at Centre-North node.

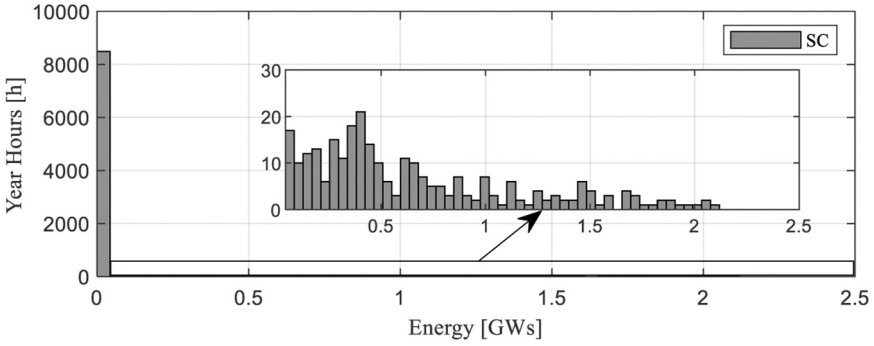

Fig. 9. Additional energy repartition at Centre-South node.

Table 6
Additional inertia: statistical indicators by source.

		SCs [GWs]	BESSs [GWs]	PV [GWs]	WTs [GWs]
NORTH	Av	286.32	13.53	11.02	0.26
	SD	127.69	1.39	21.19	0.22
CENTRE-NORTH	Av	13.73	2.82	2.18	0.35
	SD	6.17	0.43	3.86	0.36
CENTRE-SOUTH	Av	0.63	0.00	0.00	0.00
	SD	0.51	0.00	0.00	0.00

optimization algorithm results, a detailed inertial controller has been developed for these technologies, enabling them to contribute with SI [40,41].

Furthermore, each network node is equipped with two equivalent SCs, representing respectively the already-installed and newly-installed units.

The split contingency is activated 20 [s] after the system attains steady-state. The RoCoF, following the loss of the 9998.1 [MW] injection from Europe, is recorded at critical values at North, Centre-North and Centre-South nodes, as reported in Table 5 for the base scenario (i.e. with no support), with the application of the proposed approach and with the method described in [34]. Moreover, Fig. 3 depicts the time domain RoCoF profiles, with the panels showcasing the base reference scenario respectively in North, Centre-North and Centre-South market areas. A comparison between the RoCoF trends at North, Centre-North and Centre-South market areas considering ZA and AINRA results in terms of additional inertia installations is provided in Fig. 4, Fig. 5 and Fig. 6.

The minimum values reported in Table 5 highlight that the AINRA effectively constrains the RoCoF to values greater than or equal to −0.5 Hz/s, closely aligning with the defined limitation $RoCoF_{\text{lim}}$. Considering the scenario with additional inertia, Fig. 4, Fig. 5 and Fig. 6

Table 7
AINRA decision variables.

Symbol	Description
$H_{add,PV,i}$	Additional SI provided by PV power plants in market zone i
$H_{add,WT,i}$	Additional SI provided by WT power plants in market zone i
$H_{add,ST,i}$	Additional SI provided by BESS power plants in market zone i
$H_{add,SC,i}$	Additional inertia provided by additional SCs to be installed in market zone i
$H_{add,i}$	Overall additional inertia possibly necessary in market zone i to limit the zonal RoCoF
$C_{PV,i}$	Overall cost related to the provision of additional synthetic inertia by PV power plants in market zone i, dependent on $H_{add,PV,i}$
$C_{WT,i}$	Overall cost related to the provision of additional synthetic inertia by WT power plants in market zone i, dependent on $H_{add,WT,i}$
$C_{ST,i}$	Overall cost related to the provision of additional synthetic inertia by BESS power plants in market zone i, dependent on $H_{add,ST,i}$
$C_{SC,i}$	Total installation cost for additional SCs to be installed in market zone i, dependent on $H_{add,SC,i}$
$A_{PV,i}$	Rating of the PV power plants of market zone i to be integrated with a SI controller, dependent on $H_{add,PV,i}$
$A_{WT,i}$	Rating of the WT power plants of market zone i to be integrated with a SI controller dependent on $H_{add,WT,i}$
$A_{ST,i}$	Rating of the BESS power plants of market zone i to be integrated with a SI controller,$H_{add,ST,i}$
$A_{SC,i}$	Rating of new SCs to be installed in market zone i to be integrated with a SI controller dependent on $H_{add,SC,i}$

Table 8
AINRA input parameters.

Symbol	Description
N	Total number of market zones into which the transmission network is divided.
S_b	System power base
$H_{p,i}$	Physical inertia of conventional SGs and SCs already installed in 2030 at market zone i
f_n	Nominal frequency of the system
α	Converter overloading coefficient
$\cos\varphi_{\min}$	Minimum power factor to be granted by inverter-based power plants
$H_{PV,\max,i}$	Maximum SI coefficient for PV plants in market zone i
$P_{PV,i}$	active power injected by PV power plants in market zone i
$P_{curt,i}$	Total PV curtailment power at node i
$P_{PV,i,MPPT}$	MPPT power of the PV source at market zone i
$A_{PV,on,i}$	Total rating of the PV plant apparent power connected to the i-th market zone in the considered hour
$H_{WT,\max,i}$	Maximum SI coefficient for WT plants in market zone i
$P_{WT,i}$	Active power production from all the WT units connected to the i-th market zone of the network
$A_{WT,on,i}$	Apparent power of all the WT power plants connected to the i-th market zone of the network
$\Delta P_{WT,i}$	Active power for SI provision in under-frequency transients made available by WT power plants connected to the i-th market zone of the network
$H_{ST,\max,i}$	Maximum SI coefficient for BESS plants in market zone i
$P_{ST,i}$	Active power production from all the BESS power plants connected to the i-th market zone of the network
$A_{ST,on,i}$	Apparent power of all the BESS power plants connected to the i-th market zone of the network
$\Delta P_{ST,i}$	Active power for SI provision made available by BESS power plants connected to the i-th market zone of the network
k_{PV}	Unitary cost of incorporating a SI controller into a PV unit inverter, expressed in Euros per PV inverter
k_{WT}	Unitary cost related to the integration of a SI controller into a WT inverter
k_{ST}	Unitary cost of deploying an SI controller in a BESS inverter
k_{SC}	Unitary cost for the installation of a new SC
H_{SC}	Inertia constant of a single SC

show in blue the RoCoF profiles obtained with the AINRA strategy and in red those obtained with the procedure [34] (that was named as ZA). As explained before, the approach proposed in [34] aimed at constraining the RoCoF of the whole Italian network and then distributing the necessary additional inertia among the MZ with an algorithm that used as contingency this splitting of each MZ with the zones neighbouring it

Table 9
Generated power variations, hours 1804 and 1951.

	Hour 1804 ΔP_G [MW]	Hour 1951 ΔP_G [MW]
NORTH	10,523.12	10,578.37
CENTRE NORTH	615.08	608.08
CENTRE SOUTH	206.30	208.86
SOUTH	57.64	59.32
CALABRIA	4.16	4.17
SICILY	6.06	6.15

Table 10
Needed and additional inertia, hours 1804 and 1951.

	Hour 1804		Hour 1951	
	H_i [s]	$H_{add,i}$ [s]	H_i [s]	$H_{add,i}$ [s]
NORTH	526.16	445.09	528.92	467.67
CENTRE-NORTH	30.75	23.89	30.40	23.45
CENTRE SOUTH	0.00	0.00	10.44	0.032
SOUTH	0.00	0.00	0.00	0.00
CALABRIA	0.00	0.00	0.00	0.00
SICILY	0.00	0.00	0.00	0.00

Table 11
Distribution of the Additional Inertia, hours 1804.

	$H_{PV,i}$[s]	$H_{WT,i}$[s]	$H_{ST,i}$[s]	$H_{SC,i}$[s]
NORTH	0.00	0.30	13.98	430.81
CENTRE NORTH	0.00	0.50	2.96	20.43
CENTRE SOUTH	0.00	0.00	0.00	0.00
SOUTH	0.00	0.00	0.00	0.00
CALABRIA	0.00	0.00	0.00	0.00
SICILY	0.00	0.00	0.00	0.00

Table 12
Distribution of the Additional Inertia, hours 1951.

	$H_{PV,i}$[s]	$H_{WT,i}$[s]	$H_{ST,i}$[s]	$H_{SC,i}$[s]
NORTH	0.00	0.04	13.98	453.66
CENTRE NORTH	0.00	0.16	2.96	20.33
CENTRE SOUTH	0.00	0.03	0.00	0.00
SOUTH	0.00	0.00	0.00	0.00
CALABRIA	0.00	0.00	0.00	0.00
SICILY	0.00	0.00	0.00	0.00

at north. Therefore, these contingencies were not in principle consistent with the one triggering the FS at national level. On the other hand, the proposed approach basically estimates the power unbalance at each node because of the perturbation undergone at national level. The result is a different distribution of the inertia among the market zone and the fact that each individual node RoCoF is constrained to be within the desired range contrarily to what happened applying the ZA procedure.

The effectiveness of the AINRA procedure is further highlighted through additional simulations, whose several results are reported in the Appendix B.

With the successful validation of the proposed procedure, the analysis is expanded to encompass the complete set of annual data for the Italian transmission network and the ensuing results are presented in the subsequent section.

6. Statistical Results

In this section, the outcomes of the procedure presented in Section II for the entire year 2030 are presented. To facilitate understanding and readability, it was chosen to report distributions related to energy rather than inertia constant. Indeed, unlike the inertia constant, it does not need to be related to the size of the source.

Fig. 7, Fig. 8 and Fig. 9 depict the statistical distributions of the

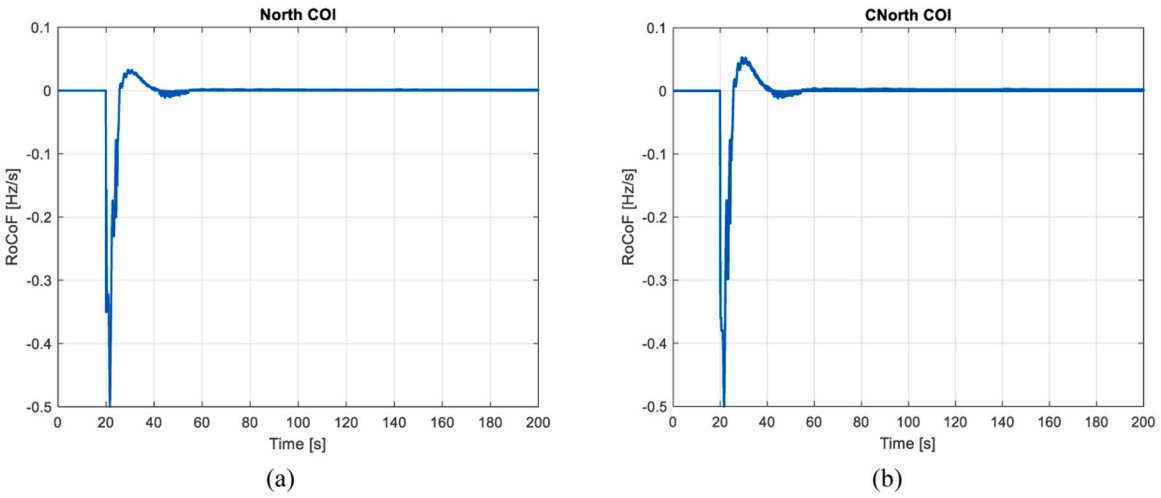

Fig. 10. RoCoF profiles with frequency support at North (a) and Centre-North (b) – AINRA, hour 1804.

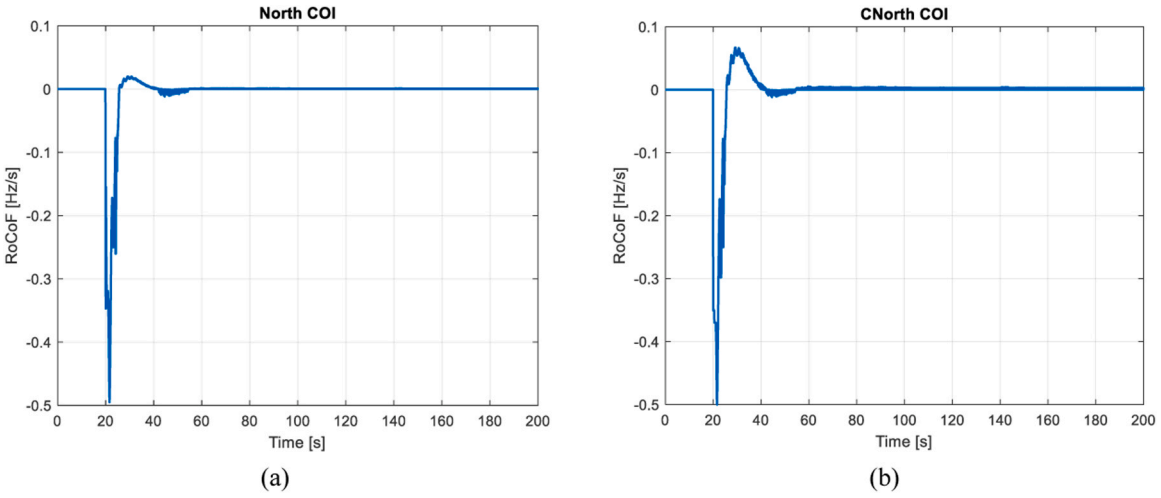

Fig. 11. RoCoF profiles with frequency support at North (a) and Centre-North (b) – AINRA, hour 1951.

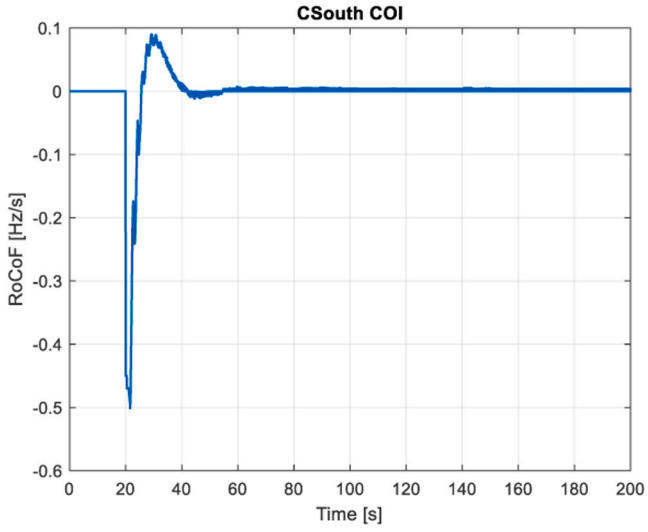

Fig. 12. RoCoF profiles with frequency support at Centre-South – AINRA, hour 1951.

energy provided by the four technologies at North, Centre-North and Centre-South. In general, photovoltaic installations do not provide inertial support for the majority of hours characterized by underfrequency transients.

This is because, as indicated by the data supplied by Terna, curtailment of PV is seldom applied and therefore they are not able to provide additional active power for the SI service. The energy profile of BESSs is contingent upon the magnitude of the perturbation and upon the capability of PV and WT systems to provide the necessary inertia for restricting RoCoF within the desired interval by their own. Analysing Fig. 7 and Fig. 8, a peak in the BESS's statistical distributions can be identified, corresponding to the last statistical class, associated with BESSs saturation conditions. In other words, this peak represents the hours during which BESSs provide the maximum SI contribution to constrain RoCoF. Even during hours when BESSs are saturated, the installation of SCs may be necessary due to the large perturbation magnitude. Lastly, the energy distribution of SCs shows a variable profile because no technological constraints are imposed on them. SCs effectively limit the nodes' RoCoF when the available inertia from other technologies is insufficient. Fig. 9 specifically illustrates the distribution of SCs, as other technologies are unable to provide any SI support at the Centre-South node.

For clarity, the outcomes of the proposed procedure are summarized in Table 6, featuring the Average (Av) and Standard Deviation (SD)

values of energy contributions from each technology within the most critical market zones. These values are computed excluding the hours during which the respective source does not contribute to the FS.

Based on Fig. 7, Fig. 8 and Fig. 9 and Table 6, it becomes apparent that, for the majority of hours, the highest additional kinetic energy capacity has to be installed at North, primarily by SCs. This phenomenon can be attributed to different reasons: firstly, SCs are the sole technology not subject to physical installation limitations and, secondly, in accordance with the proposed procedure, the generation at node North produces most of the power that was injected from Europe before the contingency. Specifically, SCs, being the costliest option, serve to support the RoCoF when the available inertia from other technologies is inadequate.

7. Conclusion

This paper addressed the challenges posed by critical frequency transients in future power systems, resulting from the increased integration of RESs. The primary focus is on mitigating variations in the RoCoF in a Transmission Network, with a specific examination of the Italian test-case scenario. The study utilizes the 2030 dataset provided by Terna, offering insights into the anticipated configuration of the Italian transmission system throughout the year 2030.

In tackling the challenge of inertia reduction from a techno-economic perspective, this paper introduced a procedure for estimating the required inertia and an optimization algorithm for its distribution. The procedure determined the additional inertia that PV, WT, BESSs, and SCs have to provide to restrict the RoCoF of each network node within a desired range. The algorithm AINRA allocated the inertia among different technologies minimizing the cost of the necessary updates/new installations.

The methodology's validation involved replicating the Italian network within the DIgSILENT PowerFactory software environment. Subsequent simulations were conducted to observe frequency transients arising from the separation between Italy and the broader EU network. Results obtained through PowerFactory simulation demonstrated the effectiveness of the proposed procedure. Subsequently, the developed method was employed to estimate the distribution of the additional inertia for each energy source and MZ.

Future developments may explore the potential inertial contribution from HVDC converters and devise a method to assess the need for short circuit power and/or reactive power to address voltage. Moreover, the proposed methodology will be applied and validated on other network topologies, assessing the impact of the topology on the reliability of the results.

CRediT authorship contribution statement

Denegri Gio Battista: Conceptualization. **Lisciandrello Giuseppe:** Resources, Data curation. **Orrù Luca:** Resources, Data curation. **Minetti Manuela:** Writing – original draft, Software, Methodology, Conceptualization. **Fresia Matteo:** Writing – original draft, Software, Methodology, Conceptualization. **Procopio Renato:** Writing – review & editing, Supervision. **Bonfiglio Andrea:** Writing – review & editing, Supervision.

Declaration of Competing Interest

The authors declare that they have no known competing financial interests or personal relationships that could have appeared to influence the work reported in this paper.

Appendix A

This Appendix aims at presenting the decision variables and the parameters involved in the AINRA optimization problem.

The unique set involved in the optimization problem is $i = 1,\ldots,N$: this set denotes the market zones into which a transmission network could be divided, where N is the total number of market zones into which the transmission network is divided.

The decision variables of the optimization problems are listed here below in Table 7.

The main input parameters of AINRA optimization problem are listed here below in Table 8.

Appendix. B

Results of the AINRA method for two additional hours, specifically hours 1804 and 1951, to further validate the results and clarify the methodology are detailed in this Appendix. Table 9 and Table 10 show the generated power variation and both the needed and the additional inertia respectively, for each hour and for each market zone. Table 11 and Table 12 report the additional inertia repartition for hours 1804 and 1951 respectively. Fig. 10, Fig. 11 and Fig. 12 represent the RoCoF profile obtained for each market zone requiring additional inertia for both the selected hours and showing the effectiveness of AINRA for RoCoF containment.

Data availability

The data that has been used is confidential.

References

[1] J. Zhou, Y. Guo, L. Yang, J. Shi, Y. Zhang, Y. Li, Q. Guo, H. Sun, A review on frequency management for low-inertia power systems: From inertia and fast frequency response perspectives, Electr. Power Syst. Res. 228 (2024) 110095.
[2] K.S. Ratnam, K. Palanisamy, G. Yang, Future low-inertia power systems: Requirements, issues, and solutions - A review, Renew. Sustain. Energy Rev. 124 (2020) 109773.
[3] M. Minetti, M. Fresia, A Review of Primary and Secondary Control for Islanded No-Inertia Microgrids, : 2021 IEEE Int. Conf. Environ. Electr. Eng. 2021 IEEE Ind. Commer. Power Syst. Eur. (EEEIC / ICPS Eur.) (2021) 1–7.
[4] M. Minetti, M. Fresia, Simplified Conditions for the Evaluation of Droop-Controlled Microgrids Stability, : 2021 12th Int. Symp. . Adv. Top. Electr. Eng. (ATEE) (2021) 1–6.
[5] J. Fang, H. Li, Y. Tang, F. Blaabjerg, On the Inertia of Future More-Electronics Power Systems, IEEE J. Emerg. Sel. Top. Power Electron. 7 (2019) 2130–2146.
[6] A.Q. Al-Shetwi, M.A. Hannan, K.P. Jern, M. Mansur, T.M.I. Mahlia, Grid-connected renewable energy sources: Review of the recent integration requirements and control methods, J. Clean. Prod. 253 (2020) 119831.
[7] V.A.V. Mohanan, I.M.Y. Mareels, R.J. Evans, R.R. Kolluri, Stabilising influence of a synchronous condenser in low inertia networks, IET Gener., Transm. Distrib. 14 (2020) 3582–3593.
[8] A. Roux, B. Bekker, A. Dalton, Synchronous condensers as a viable inertia support mechanism on the future South African grid, Energy Sustain. Dev. 69 (2022) 192–201.
[9] J. Dhanuja Lekshmi, Z.H. Rather, B.C. Pal, Frequency Response Improvement in RE Integrated Low Inertia Power Systems using Synchronous Condensers, in: 2022 22nd National Power Systems Conference, NPSC 2022, 2022, pp. 602-607.
[10] M.I. Pereira, C. Moreira, Improving Stability of Reduced Inertia Transmission Systems, in: 2024 IEEE 22nd Mediterranean Electrotechnical Conference, MELECON 2024, 2024, pp. 443-448.
[11] A. Fernández-Guillamón, E. Gómez-Lázaro, E. Muljadi, Á. Molina-Garcia, A review of virtual inertia techniques for renewable energy-based generators, Renew. Energy–Technol. Appl. (2021).
[12] Y. Qi, H. Deng, X. Liu, Y. Tang, Synthetic inertia control of grid-connected inverter considering the synchronization dynamics, IEEE Trans. Power Electron. 37 (2021) 1411–1421.
[13] T. Kerdphol, F.S. Rahman, M. Watanabe, Y. Mitani, Virtual inertia synthesis and control, Springer, 2021.
[14] P. Kushwaha, V. Prakash, R. Bhakar, U.R. Yaragatti, Synthetic inertia and frequency support assessment from renewable plants in low carbon grids, Electr. Power Syst. Res. 209 (2022) 107977.
[15] R. Ghosh, N.R. Tummuru, B.S. Rajpurohit, A. Monti, Virtual inertia from renewable energy sources: Mathematical representation and control strategy, in: 2020 IEEE International Conference on Power Electronics, Smart Grid and Renewable Energy (PESGRE2020), IEEE, 2020, pp. 1-6.
[16] A. Berizzi, A. Bosisio, V. Ilea, D. Marchesini, R. Perini, A. Vicario, Analysis of synthetic inertia strategies from wind turbines for large system stability, IEEE Trans. Ind. Appl. 58 (2022) 3184–3192.
[17] S. Fathallah, X. Liu, H.M. Rashad, A.H. Besheer, New Synthetic Inertia Control for Wind Energy Conversion System, IEEE Access (2023).

[18] D.M. Magnus, C.C. Scharlau, L.L. Pfitscher, G.C. Costa, G.M. Silva, A novel approach for robust control design of hidden synthetic inertia for variable speed wind turbines, Electr. Power Syst. Res. 196 (2021) 107267.
[19] R. Villena-Ruiz, A. Honrubia-Escribano, J.C. Hernández, E. Gómez-Lázaro, Assessment of the synthetic inertial response of an actual solar PV power plant, Int. J. Electr. Power Energy Syst. 157 (2024) 109875.
[20] P. Saxena, N. Singh, A.K. Pandey, Self-regulated solar PV systems: Replacing battery via virtual inertia reserve, IEEE Trans. Energy Convers. 36 (2021) 2185–2194.
[21] Q. Lei, F. Arraño-Vargas, G. Konstantinou, Adaptive Power Reserve Control for Photovoltaic Power Plants Based on Local Inertia in Low-Inertia Power Systems, IEEE J. Emerg. Sel. Top. Ind. Electron. (2023).
[22] M. Minetti, M. Fresia, D. Mestriner, An MPC approach for a PV-BESS islanded system primary regulation. IEEE International Conference on Environment and Electrical Engineering and 2021 IEEE Industrial and Commercial Power Systems Europe (EEEIC/I&CPS Europe), IEEE, 2021, pp. 1–6, https://doi.org/10.1109/EEEIC/ICPSEurope51590.2021.9584533.
[23] C.E. Okafor, K.A. Folly, Provision of Additional Inertia Support for a Power System Network Using Battery Energy Storage System (BESS), IEEE Access (2023).
[24] F. You, X. Si, R. Dong, D. Lin, Y. Xu, Y. Xu, A State-of-Charge-Based Flexible Synthetic Inertial Control Strategy of Battery Energy Storage Systems, Front. Energy Res. 10 (2022).
[25] A. Criollo, L.I. Minchala-Avila, D. Benavides, P. Arévalo, M. Tostado-Véliz, D. Sánchez-Lozano, F. Jurado, Enhancing Virtual Inertia Control in Microgrids: A Novel Frequency Response Model Based on Storage Systems, Batteries 10 (2024).
[26] D. Curto, S. Favuzza, V. Franzitta, A. Guercio, M.Amparo Navarro Navia, E. Telaretti, G. Zizzo, Grid Stability Improvement Using Synthetic Inertia by Battery Energy Storage Systems in Small Islands, Energy 254 (2022) 124456.
[27] H. Gu, R. Yan, T.K. Saha, E. Muljadi, J. Tan, Y. Zhang, Zonal inertia constrained generator dispatch considering load frequency relief, IEEE Trans. Power Syst. 35 (2020) 3065–3077.
[28] H. Gu, R. Yan, T.K. Saha, Minimum synchronous inertia requirement of renewable power systems, IEEE Trans. Power Syst. 33 (2017) 1533–1543.
[29] N. Holjevac, T. Baškarad, J. Đaković, M. Krpan, M. Zidar, I. Kuzle, Chall. High. Renew. Energy Sources Integr. Power Syst. — Case Croat. 14 (2021) 1047.
[30] M. Eidiani, Modeling renewable energy resources using DIgSILENT PowerFactory software, : Power Syst. Oper. 100% Renew. Energy Sources (2023) 165–202.
[31] S. Im, K. Lee, B. Lee, Estimation of maximum non-synchronous generation of renewable energy in the South Korea power system based on the minimum level of inertia, IET Renew. Power Gener. 18 (2024) 1260–1268.
[32] M. Fresia, M. Minetti, A. Bonfiglio, R. Procopio, G. Lisciandrello, L. Orrù, RoCoF Mitigation in the Italian Transmission Network: a Methodology for Inertia Optimization, in: IEEE 22nd Mediterranean Electrotechnical Conference (MELECON), 2024, pp. 424–429, https://doi.org/10.1109/MELECON56669.2024.10608532.
[33] A. Bonfiglio, M. Fresia, M. Minetti, R. Procopio, A. Rosini, G. Lisciandrello, L. Orrù, Inertia Requirements Assessment for the Italian Transmission Network in the Future Network Scenario. in: 2023 IEEE Belgrade PowerTech, IEEE, 2023, pp. 1–5.
[34] M. Fresia, M. Minetti, A. Rosini, R. Procopio, A. Bonfiglio, M. Invernizzi, G. B. Denegri, G. Lisciandrello, L. Orrù, A Techno-Economic Assessment to Define Inertia Needs of the Italian Transmission Network in the 2030 Energy Scenario, IEEE Trans. Power Syst. (2023) 1–12.
[35] O. Ajala, A. Domínguez-García, P. Sauer, D. Liberzon, A Library of Second-Order Models for Synchronous Machines, IEEE Trans. Power Syst. 35 (2020) 4803–4814.
[36] M. Fresia, M. Minetti, R. Procopio, A. Bonfiglio, G. Lisciandrello, L. Orrù, Load Flow Assignments' Definition from Day-Ahead Electricity Market Interconnection Power Flows: A Study for Transmission Networks, : Energ. (2024).
[37] Terna, Piano di Sviluppo della Rete, in, 2023.
[38] F.M. Gonzalez-Longatt, J.L. Rueda, PowerFactory applications for power system analysis, Springer, 2014.
[39] J. Rocabert, A. Luna, F. Blaabjerg, P. Rodríguez, Control of power converters in AC microgrids, IEEE Trans. Power Electron. 27 (2012) 4734–4749.
[40] F. Gonzalez-Longatt, E. Chikuni, E. Rashayi, Effects of the synthetic inertia from wind power on the total system inertia after a frequency disturbance, in: 2013 IEEE International Conference on Industrial Technology (ICIT), IEEE, 2013, pp. 826-832.
[41] A. Bonfiglio, M. Lodi, A. Rosini, A. Oliveri, R. Procopio, Design, realization and testing of a synthetic inertia controller for wind turbine power generators, Sustain. Energy, Grids Netw. 38 (2024).